



Journal of Geophysical Research: Atmospheres

RESEARCH ARTICLE

10.1002/2015JD024703

Special Section:

Deep Convective Clouds and Chemistry 2012 Studies (DC3)

Key Points:

- NASA LNOM and radar combined provide a useful new approach for studying the dynamical control of lightning properties and LNO_X
- Flash extent and NO_X production are not as well correlated to dynamical properties as flash rate
- Majority of NO_X production is from ground flashes despite larger cloud flash extent and rates

Correspondence to:

L. D. Carey, larry.carey@nsstc.uah.edu

Citation:

Carey, L. D., W. Koshak, H. Peterson, and R. M. Mecikalski (2016), The kinematic and microphysical control of lightning rate, extent, and NO_X production, *J. Geophys. Res. Atmos.*, *121*, 7975–7989, doi:10.1002/2015JD024703.

Received 22 DEC 2015 Accepted 20 JUN 2016 Accepted article online 23 JUN 2016 Published online 12 JUL 2016

The kinematic and microphysical control of lightning rate, extent, and NO_X production

Lawrence D. Carey¹, William Koshak², Harold Peterson³, and Retha M. Mecikalski¹

¹Department of Atmospheric Science, University of Alabama in Huntsville, Huntsville, Alabama, USA, ²Earth Science Office, NASA Marshall Space Flight Center, Huntsville, Alabama, USA, ³Bureau of Indian Affairs, Eastern Region Office, Nashville, Tennessee, USA

Abstract This study investigates the kinematic and microphysical control of lightning properties, particularly those that may govern the production of nitrogen oxides $(NO_X = NO + NO_2)$ via lightning (LNO_X), such as flash rate, type, and extent. The NASA Lightning Nitrogen Oxides Model (LNOM) is applied to lightning observations following multicell thunderstorms through their lifecycle in a Lagrangian sense over Northern Alabama on 21 May 2012 during the Deep Convective Clouds and Chemistry (DC3) experiment. LNOM provides estimates of flash rate, type, channel length distributions, channel segment altitude distributions (SADs), and LNO_x production profiles. The LNOM-derived lightning characteristics and LNO_x production are compared to the evolution of radar-inferred updraft and precipitation properties. Intercloud, intracloud (IC) flash SAD comprises a significant fraction of the total (IC + cloud-to-ground [CG]) SAD, while increased CG flash SAD at altitudes >6 km occurs after the simultaneous peaks in several thunderstorm properties (i.e., total [IC + CG] and IC flash rate, graupel volume/mass, convective updraft volume, and maximum updraft speed). At heights < 6 km, the CG LNO $_X$ production dominates the column-integrated total LNO_X production. Unlike the SAD, total LNO_X production consists of a more equal contribution from IC and CG flashes for heights >6 km. Graupel volume/mass, updraft volume, and maximum updraft speed are all well correlated to the total flash rate (correlation coefficient, $\rho \ge 0.8$) but are less correlated to total flash extent ($\rho \ge 0.6$) and total LNO_X production ($\rho \ge 0.5$). Although LNOM transforms lightning observations into LNO_X production values, these values are estimates and are subject to further independent validation.

1. Introduction

The Deep Convective Clouds and Chemistry (DC3) experiment seeks to quantify the relationships between storm physics, dynamics, lightning characteristics, and the production of nitrogen oxides ($NO_X = NO + NO_2$) via lightning (LNO_X) [Barth et al., 2015]. Ultimately, these relationships can be used to parameterize LNO_X in numerical cloud models lacking explicit prediction of cloud electrical and lightning processes [e.g., Pickering et al., 1998; Barthe and Barth, 2008; Barthe et al., 2010]. The focus of this study is to investigate the kinematic and microphysical control of lightning properties, particularly those that may govern LNO_X production, such as flash rate, type [i.e., intracloud, intercloud, or cloud-to-air (all referred to as IC flashes) versus cloud-to-ground (CG)] and extent across northern Alabama during DC3. Prior studies have demonstrated that lightning flash rate and type are correlated to kinematic and microphysical properties in the mixed-phase region of thunderstorms, such as updraft volume and graupel mass (Goodman et al. [1988], Carey and Rutledge [1996] (hereafter CR96), Jameson et al. [1996], Bringi et al. [1997], Carey and Rutledge [2000] (hereafter CR00), Lang and Rutledge [2002], Schumann and Huntrieser [2007], Deierling et al. [2008], Deierling and Petersen [2008], Mecikalski et al. [2015] (hereafter MEA15), and many more).

More study is required to generalize these relationships in a wide variety of storm modes and meteorological conditions. Less is known about the coevolving relationship between storm physics, morphology, and three-dimensional flash extent, despite its obvious importance for LNO $_X$ production. To address this conceptual gap, the NASA Lightning Nitrogen Oxides Model (LNOM) is applied to North Alabama Lightning Mapping Array (NALMA) and Vaisala National Lightning Detection NetworkTM (NLDN) observations following ordinary convective cells through their lifecycle. LNOM provides estimates of flash rate, flash type, channel length distributions, lightning channel segment altitude distributions (SADs), and LNO $_X$ production profiles [Koshak, 2014; Koshak et al., 2014]. For this study, LNOM is applied in a Lagrangian sense to a multicell thunderstorm over Northern Alabama on 21 May 2012 during DC3 in which aircraft observations of NO $_X$ are available.

©2016. American Geophysical Union. All Rights Reserved.



However, it is important to note that these aircraft observations are not usable for comparison to the storm analyzed here because of the following reasons: (1) The NASA DC-8 aircraft only sampled the storm for 13 min (from 2117 to 2130 UTC) with one loop through the anvil at one altitude (11.5 km), which is not sufficient to characterize lightning NO_X production and (2) the National Science Foundation/National Center for Atmospheric Research Gulfstream-V (NSF/NCAR-GV) aircraft only sampled downwind of the storm at 10 km for 25 min (from 2050 to 2115 UTC), but smaller NO_X values were found close to the storm than farther downwind, indicating the likely influence of other upwind storms, thus making these observations unusable for an LNO_X analysis for the storm of interest [Pollack et al., 2016]. In addition, other members of the DC3 group have, and are currently in the process of analyzing storms in Colorado, Oklahoma, and Alabama and are either using the LNO $_X$ observations to develop a measurement-based range for NO $_X$ production (such as Pollack et al. [2016]) or doing Weather Research and Forecasting (WRF) modeling coupled with chemistry (i.e., WRF-Chem modeling [Li et al., 2014, 2016]) and therefore it was decided to not duplicate this work. Also, this study closely follows that of MEA15 in that the same convective storm, together with the same dual-Doppler radar, NALMA and NLDN data are used. The main difference with this study is that we compare the LNOM lightning characteristics and LNO_X production estimates to the *inferred updraft* and *precipitation properties* obtained from the MEA15 study. The goal of this paper is to understand how radar-derived variables (such as radar reflectivity, graupel volume, graupel mass, and updraft volume) compare and correlate to output from the LNOM model. Therefore, this paper is focused on trying to improve our understanding of how LNOM lightning properties and LNO_X production rates are related to storm kinematic and microphysical processes. As there are few studies that have compared radar-derived kinematic and microphysical information to the full breadth of lightning properties available from the LNOM (e.g., flash rate, flash type, profile of flash extent, and profiles of LNO_X production), this study provides a unique contribution to the literature that, along with ongoing DC3 WRF-Chem modeling and aircraft in situ studies mentioned above, will help further our understanding of the integrated kinematic-microphysical-chemical properties of thunderstorms.

2. Background

Based on numerous laboratory [e.g., *Takahashi*, 1978; *Saunders*, 1994; *Saunders and Peck*, 1998] and observational [*Dye et al.*, 1986, 1989] studies, the primary means for particle charging in thunderstorms is thought to be a noninductive mechanism, which involves rebounding collisions between graupel and small ice crystals in the presence of supercooled water. Particle fall speed differences and convective motions in a vigorous updraft result in storm scale charge separation and strong electric fields sufficient for breakdown and lightning. Because of its ability to identify and quantify graupel and convective updrafts, dual-polarization and multi-Doppler radar have been used to study the microphysical and kinematic control of lightning flash rate (e.g., CR96; CR00, *Wiens et al.* [2005], *Deierling et al.* [2008], *Deierling and Petersen* [2008], and MEA15, among others). In these studies, graupel amount (e.g., graupel echo volume or precipitation ice mass) and updraft strength (e.g., maximum updraft, updraft volume) were shown to be highly correlated to the total (IC+CG) lightning flash rate.

Less has been documented regarding the kinematic and microphysical control of flash extent. *Bruning and MacGorman* [2013] presented data from supercells that support their theoretical prediction from electrostatics that frequent breakdown and large flash extents are opposed. In *Bruning and MacGorman* [2013] and prior studies [e.g., *Carey et al.*, 2005; *Kuhlman et al.*, 2009; *Weiss et al.*, 2012], high flash rates characterized by small extents were located near the updraft region, while large flashes tended to occur infrequently away from the convective updraft and within the stratiform precipitation or anvil region of mesoscale convective systems and supercells, respectively. The correspondence between kinematic and electrical energy spectra in *Bruning and MacGorman* [2013] suggests that advection of charge-bearing precipitation by the storm's flow, including in turbulent eddies, couples the kinematic and electrical properties of a thunderstorm, including presumably flash extent. MEA15 demonstrated that the flash sizes were larger (smaller) when the flash rates were lower (higher) in a multicellular storm. Smaller (larger) flash sizes were collocated with stronger (weaker) updrafts in the ordinary storms, a quasi-linear convective system and a supercell studied in *Schultz et al.* [2015]. In the analysis of Sao Paulo Lightning Mapping Array (SPLMA) data by *Chronis et al.* [2015], the mean horizontal and vertical flash extents each attained a maximum (minimum) around local sunrise (afternoon; i.e., 13:00–17:00 local solar time).



Lightning flash rate, size, and type are important, as these properties (among others) are thought to control the production of LNO_X [e.g., Price et al., 1997; Pickering et al., 1998; Wang et al., 1998; Schumann and Huntrieser, 2007; Barthe and Barth, 2008; Cooray et al., 2009; Peterson et al., 2009, 2010; Barthe et al., 2010; Koshak et al., 2014, 2015]. In most modeling studies, LNO $_X$ production is based on the total lightning flash rate [e.g., Pickering et al., 1998; Barthe and Barth, 2008]. However, there is some disagreement in the literature as to whether CG lightning produces the same, more, or less LNO_X than IC lightning on a per flash basis [Gallardo and Cooray, 1996; Gallardo and Rodhe, 1997; Price et al., 1997; Pickering et al., 1998; DeCaria et al., 2000; Dye et al., 2000; Fehr et al., 2004; DeCaria et al., 2005; Ridley et al., 2005; Ott et al., 2007; Schumann and Huntrieser, 2007; Barthe and Barth, 2008; Ott et al., 2010; Koshak, 2014; Koshak et al., 2014]. Price et al. [1997], Pickering et al. [1998], Koshak et al. [2014], and others suggest that there is roughly an order of magnitude difference in LNO_x production between CG and IC flashes; while DeCaria et al. [2000, 2005], Ott et al. [2007], and others suggest that CG and IC flashes may produce approximately the same amount of LNO_X per flash. With respect to this debate, it is worth pointing out that the physical characteristics of lightning (e.g., channel current, channel length, and channel altitude) substantially vary from flash to flash, so that NO_X production varies appreciably between flashes in general (even if they are of the same type, IC or CG). In addition, one also has to consider whether or not a CG does or does not have a significant in-cloud IC component. The benefit of applying LNOM is that estimates of LNO_X production are made on a flash-by-flash basis, rather than by assigning each flash (or flash type) a constant production value.

3. Data and Methodology

In order to explore the coevolving relationship between storm kinematics, microphysics, lightning properties, and LNO_X production in ordinary convection, the NASA LNOM is applied to NALMA and NLDN lightning observations and compared to multi-Doppler and polarimetric radar observations of a multicell cluster on 21 May 2012 over northern Alabama taken during the DC3 field experiment [Bain, 2013; Bain et al., 2013; Barth et al., 2015; MEA15]. In an effort to not duplicate information regarding the data and methodology used in this research, the reader is referred to Barth et al. [2015] and MEA15 as well as references therein for an in-depth discussion on the DC3 experimental design within the Alabama domain, including the quality control and data analysis procedures that were used for the radar and lightning data sets. However, relevant information that is important for understanding the analysis and results herein will be repeated here.

Two polarimetric weather radars, located ~70 km from each other, were used in this study: (1) the Advanced Radar for Meteorological and Operational Research (ARMOR) located at the Huntsville International Airport (KHSV) and coowned by the University of Alabama in Huntsville (UAH) and WHNT-TV in Huntsville, Alabama [*Petersen et al.*, 2005] and (2) the WSR-88D located at Hytop, Alabama (KHTX) (refer to Figure 1 of MEA15). ARMOR is a C-band radar (5.5 cm) while KHTX is an S-band radar (10.71 cm) [*Petersen et al.*, 2005]. Particle identification using fuzzy logic was performed on the radar data to determine hydrometeor type [*Vivekanandan et al.*, 1999; *Straka et al.*, 2000; *Deierling et al.*, 2008]. The graupel and small hail categories were used for this study in order to calculate the graupel volume and mass in the mixed-phase region located between -10° C and -40° C (roughly 6 to 10 km AGL). A multi-Doppler wind synthesis was also performed to obtain updraft velocities as well as the convective updraft (>5 m s⁻¹) volume within the mixed-phase region during the storm's lifecycle [*Miller and Frederick*, 1998]. NALMA very high frequency (VHF) source data and NLDN return stroke data were used to obtain a detailed representation of the total lightning (IC + CG) that occurred during the storm's lifecycle [*Koshak et al.*, 2004; *Goodman et al.*, 2005; *McCaul et al.*, 2005].

The NASA LNOM [Koshak, 2014; Koshak et al., 2014] ingests lightning VHF source location and time-of-occurrence LMA data that have been processed by the McCaul et al. [2005] clustering algorithm. It also ingests location, time-of-occurrence, peak current, and stroke multiplicity data from the NLDN. These data are used to determine the flash type (CG or IC, using NLDN) of each flash occurring within the LNOM analysis cylinder (height 0–20 km and variable radius). A Lagrangian (i.e., storm following) analysis cylinder of variable radius was subjectively drawn around the storm cluster of interest centered at each radar volume time (Figure 1) in order to compare the evolution of LNOM output properties to the radar observations. The LNOM analyzes the VHF sources to estimate the total channel length of each flash. Both CG and IC flashes are analyzed. LNOM slices each portion of a flash contained in the analysis cylinder into 10 m segments and sums these segments in each 100 m layer to determine the Segment Altitude Distribution (SAD) within the cylinder. The SADs are

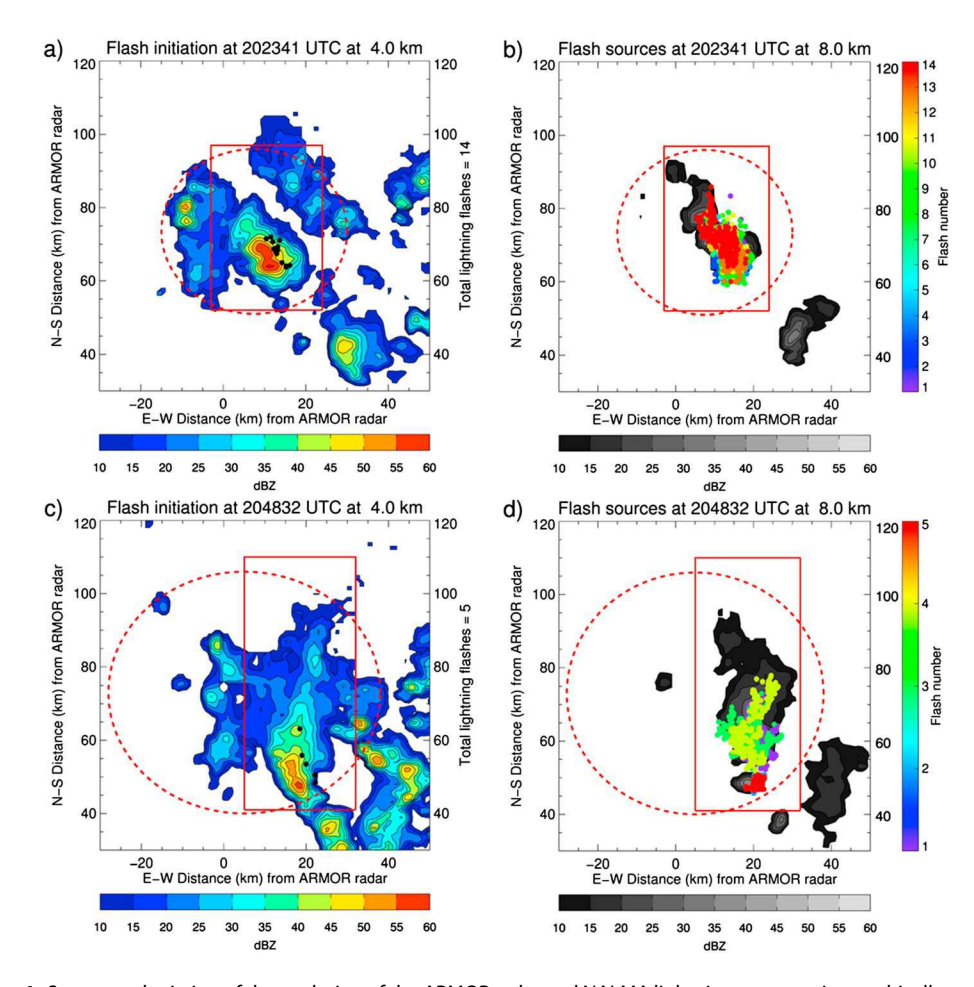


Figure 1. Summary depiction of the evolution of the ARMOR radar and NALMA lightning structure in a multicell storm cluster on 21 May 2012 at (a, b) 2023 UTC and (c, d) 2048 UTC. (left) Radar reflectivity (dBZ, color shaded) at 4 km (~ -5 °C) and NALMA flash initiation points (black dots) (Figures 1a and 1c) and (right) radar reflectivity (dBZ grey shade) at 8 km (~ -28 °C) and NALMA VHF sources associated with individual flashes (color coded by flash) (Figures 1b and 1d). The solid red box and the dashed circle depict the radar analysis domain and LNOM analysis cylinder, respectively.

summed over altitude to estimate flash extent (therefore, the flash extent is essentially the accumulated channel length within a given period, as calculated by LNOM). Finally, LNOM computes the vertical LNO $_X$ production profile from observed lightning properties in the cylinder using model parameterizations based on laboratory [*Wang et al.*, 1998; *Peterson et al.*, 2009] and theoretical [*Cooray et al.*, 2009] studies. Details on lightning channel length estimation and LNO $_X$ production parameterization in the NASA LNOM can be found in *Koshak* [2014] and *Koshak et al.* [2014]. In brief, the LNOM systematically parameterizes LNO $_X$ production associated with each 10 m channel segment. The NO $_X$ production from return strokes (based on *Wang et al.* [1998]) is calculated using peak current and multiplicity (number of strokes in a flash) information from NLDN data, and air density (channel segment altitude) is obtained using LMA VHF source altitude data. The NO $_X$ production from processes other than return strokes [*Cooray et al.*, 2009, 2012] have been included in LNOM (i.e., hot core of stepped leaders, stepped leader corona sheath, hot core of dart leaders, K changes, continuing currents, and associated M components).

4. Results

For this study, the evolution of a multicell convective cluster observed in Northern Alabama on 21 May 2012 was analyzed from 1953 to 2104 UTC using radar and lightning observations (Figure 1) and the NASA LNOM. Storm-integrated summary profiles of LNOM SAD and LNO_X production during the roughly 1 h period on 21 May 2012 are first presented followed by time-height cross sections of storm integrated SAD and LNO_X

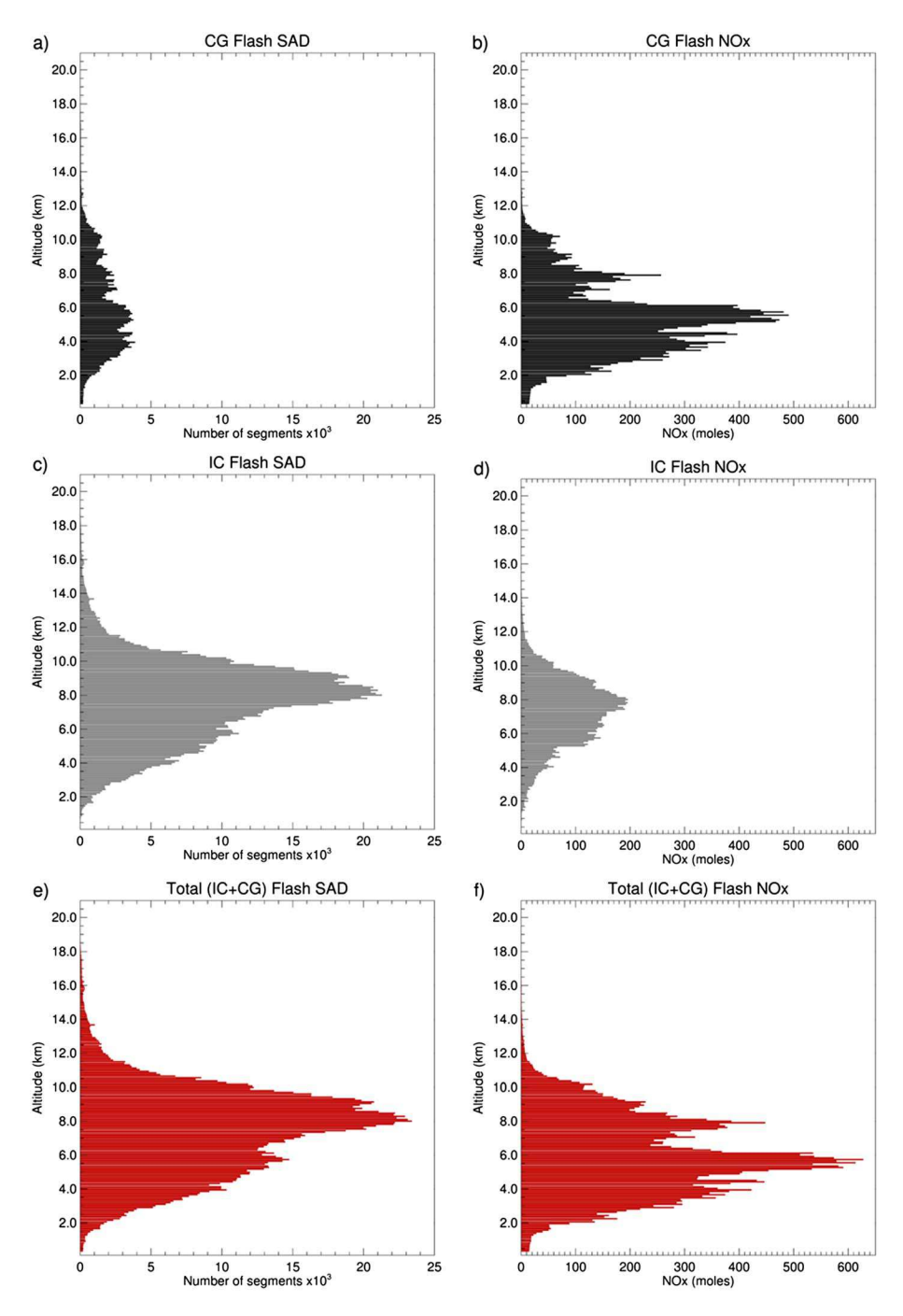


Figure 2. Storm-integrated vertical profiles of lightning extent (SAD) and LNO_X production inferred from the LNOM following a multicell storm cluster on 21 May 2012 from 1953 to 2104 UTC. (a, c, and e) SAD profiles (kilosegments) and (b, d, and f) LNO_X production profiles (moles) for CG lightning only (Figures 2a and 2b; black), IC lightning only (Figures 2c and 2d; gray), and total (IC + CG) lightning (Figures 2e and 2f; red).

production (section 4.1). Time-height cross sections of maximum reflectivity, graupel echo volume, graupel mass, and convective (>5 m s $^{-1}$) updraft volume in the charging zone are then presented for comparison with the LNOM profile properties (section 4.2). The time series of storm integrated LNOM SAD and LNO $_X$ production profiles are then carefully compared to the time series evolution of radar-inferred graupel echo volume, convective updraft volume, and graupel mass in the mixed-phase zone (sections 4.3 and 4.4). In each case, the Pearson correlation coefficient between the time series of radar and LNOM properties are



computed to quantify the potential kinematic and microphysical control of flash rate, flash extent and LNO_X production.

4.1. LNOM SAD and LNO_X Production

In order to characterize the vertical structure of lightning extent and associated production of LNO_X during the 1 h period, profiles of storm integrated LNOM SAD (left column) and LNO_X production (right column) are presented in Figure 2 for CG, IC, and total flashes (IC + CG; see figure caption for additional information). The SAD for CG flashes (Figure 2a) is significantly smaller than the IC SAD (Figure 2c) and is somewhat multimodal with several relative maxima in the vertical and dominant peaks between ~4 and 6 km altitude. The IC flash SAD has a dominant peak at 8 to 10 km altitude with a less pronounced shelf at 6 km (Figure 2c), while the total (IC + CG) SAD (Figure 2e) is clearly dominated by the IC SAD. As expected, there are more 10 m lightning segments at low levels in CG flashes in a relative sense than in IC flashes. In an absolute sense, IC lightning tends to dominate the SAD at nearly all levels except at the lowest levels (e.g., <3 km) where CG and IC flash extents are comparable.

The LNO_X production for CG flashes (Figure 2b) has a clear peak at 6 km, with secondary peaks at 8 km and roughly 4 km. The LNO_X production of IC flashes has a clear peak at 8 km with a broader maximum between 6 and 10 km, beyond which the LNO_X drops rapidly in both directions (Figure 2d). Despite dominating the SAD, the IC LNO_X production peak at 8 km is less than the corresponding CG LNO_X production peak at 6 km (Figure 2b). The CG LNO_X production is generally larger than the IC LNO_X production at all altitudes. The total (IC+CG) LNO_X production in all flashes is multimodal with a dominant peak at 6 km and secondary peaks around 4 km and 8 km altitudes (Figure 2f) and is clearly dominated by the CG LNO_X .

Time-height cross sections of LNOM SAD (left column) are provided in Figure 3 for CG flashes (Figure 3a), IC flashes (Figure 3c) and total (IC + CG) flashes (Figure 3e). Both IC and CG lightning flashes begin around 2007 UTC. Total and IC lightning SAD rapidly increases by 2015 UTC, reaching a maximum around 2024 UTC, especially aloft in the charging region between 6 km and 10 km. The total and IC lightning SAD decrease somewhat between 2024 and 2037 UTC and then increases again to a relative maximum at 2042 UTC, especially in the charging zone. The total and IC lightning SAD decrease again after 2049 UTC until they reach a final relative maximum at about 2056 UTC. After 2056 UTC, the total and IC lightning SAD decrease as the storm cluster weakens and lightning activity ceases by 2104 UTC. As noted above, the IC flash SAD dominates the total lightning flash SAD as Figures 2c and 2e are very similar in appearance, especially at altitudes above 6 km. At lower levels (<6 km), the CG flash SAD (Figure 2a) contributes more significantly to the total lightning SAD (Figure 2e). SAD associated with CG flashes is more uniformly continuous during the roughly 1 h life cycle of this storm cluster.

One notable trend in the CG activity (Figure 3a) is the increase in CG flash SAD in the charging zone aloft at altitudes >6 km after the peak in total and IC lightning SAD (Figure 3c) at 2024 UTC. VHF sources associated with these flashes typically start at >6 km altitude yet have an associated NLDN detected CG flash location. Although these flashes are categorized as CG flashes by the LNOM, it is important to note that the LNOM computes not only all the LNO $_X$ associated with the return stroke to ground (including from stepped leader, dart leader, continuing current, and M-component processes), but also any LNO $_X$ production from IC components [Koshak, 2014]. The LNO $_X$ production from the IC components of the CGs are computed just as is the LNO $_X$ production from regular ICs. This is necessary because it is likely that most CGs have at least some IC component activity. Hence, so-called IC-CG hybrid flashes [e.g., Thomas et al., 2003; Matthee and Carey, 2014] that have clear/pronounced IC components are completely handled by the general framework of the LNOM. In this multicell storm cluster, such CG flashes with initial VHF source and extensive SAD at altitudes >6 km have the largest flash extent on average of all flash types [Matthee and Carey, 2014; MEA15].

Time-height cross sections of LNO_X production (right column) are provided in Figure 3 for CG flashes (Figure 3b), IC flashes (Figure 3d), and total (IC + CG) flashes (Figure 3f). Unlike SAD, total LNO_X production is a more equal combination of IC and CG LNO_X production at heights above 6 km. At 6 km and below, the CG LNO_X production dominates the total lightning LNO_X production. The column integrated CG LNO_X production dominates the column integrated total LNO_X production with both quantities peaking broadly between 2021 UTC and 2038 UTC (overall peak at 2027 UTC) and again more sharply at 2045 UTC. Similar to the IC SAD, the IC LNO_X production peaks at 2024 UTC with secondary maxima at 2042, 2049, and 2056 UTC.

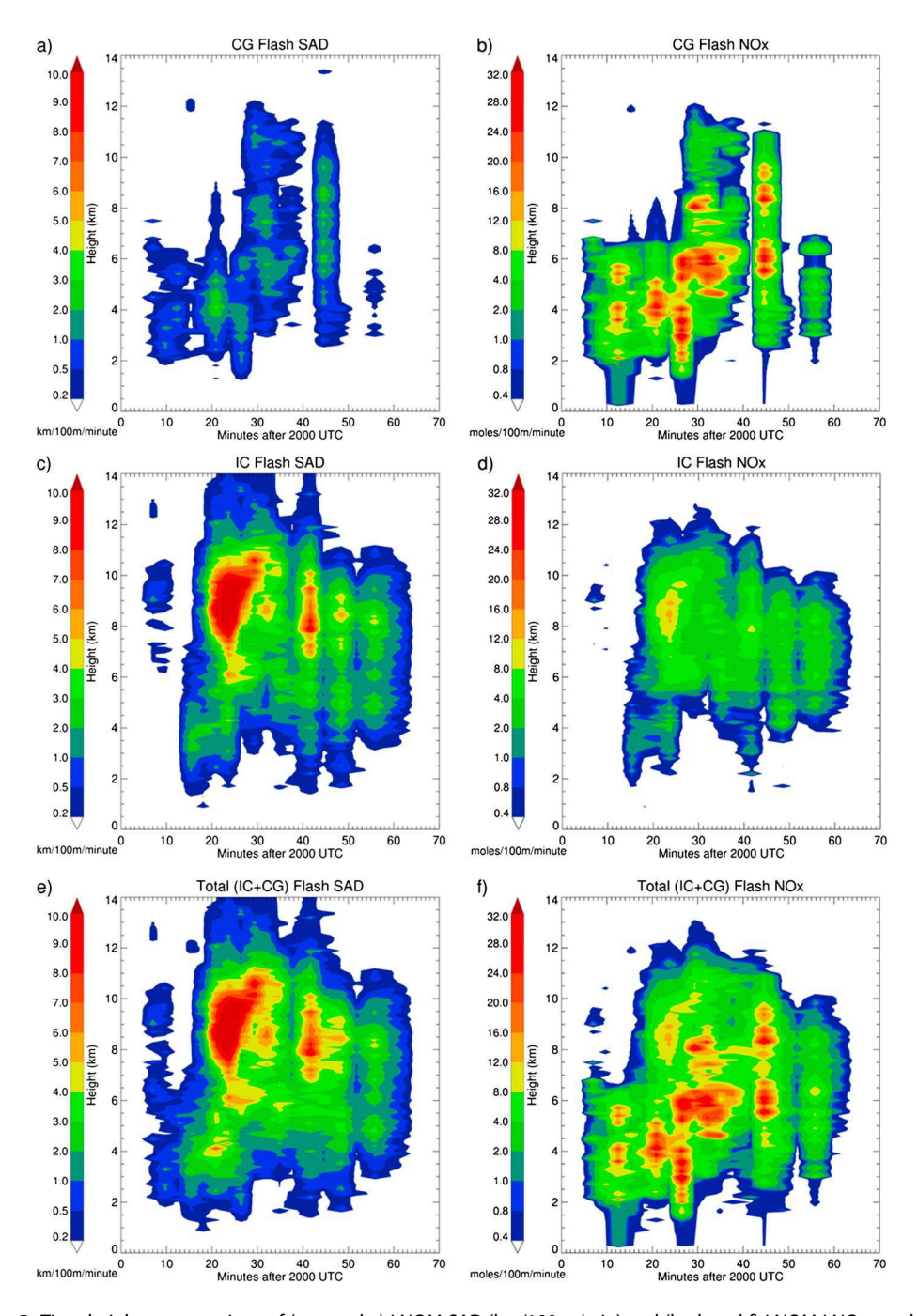


Figure 3. Time-height cross sections of (a, c, and e) LNOM SAD (km/100 m/min) and (b, d, and f) LNOM LNO $_{\rm X}$ production (moles/100 m/min) for CG lightning only (Figures 3a and 3b), IC lightning only (Figures 3c and 3d), and total (IC + CG) lightning (Figures 3e and 3f). Time is in minutes after 2000 UTC.

4.2. Radar Kinematic and Microphysical Properties

Time-height cross sections of maximum reflectivity (Figure 4a), graupel volume (Figure 4b), graupel mass (Figure 4c), and updraft volume (Figure 4d) are provided for comparison with the LNOM SAD and LNO $_X$ production. Maximum reflectivity is shown for all heights (i.e., 0–14 km) while graupel volume, graupel mass, and updraft volume are only shown in the charging zone ($-10^{\circ}\text{C} < T < -40^{\circ}\text{C}$), roughly from 6 to 10 km. The reader may also refer to Figures 7–9 of MEA15 for plots of the evolution of these same column integrated variables with time.

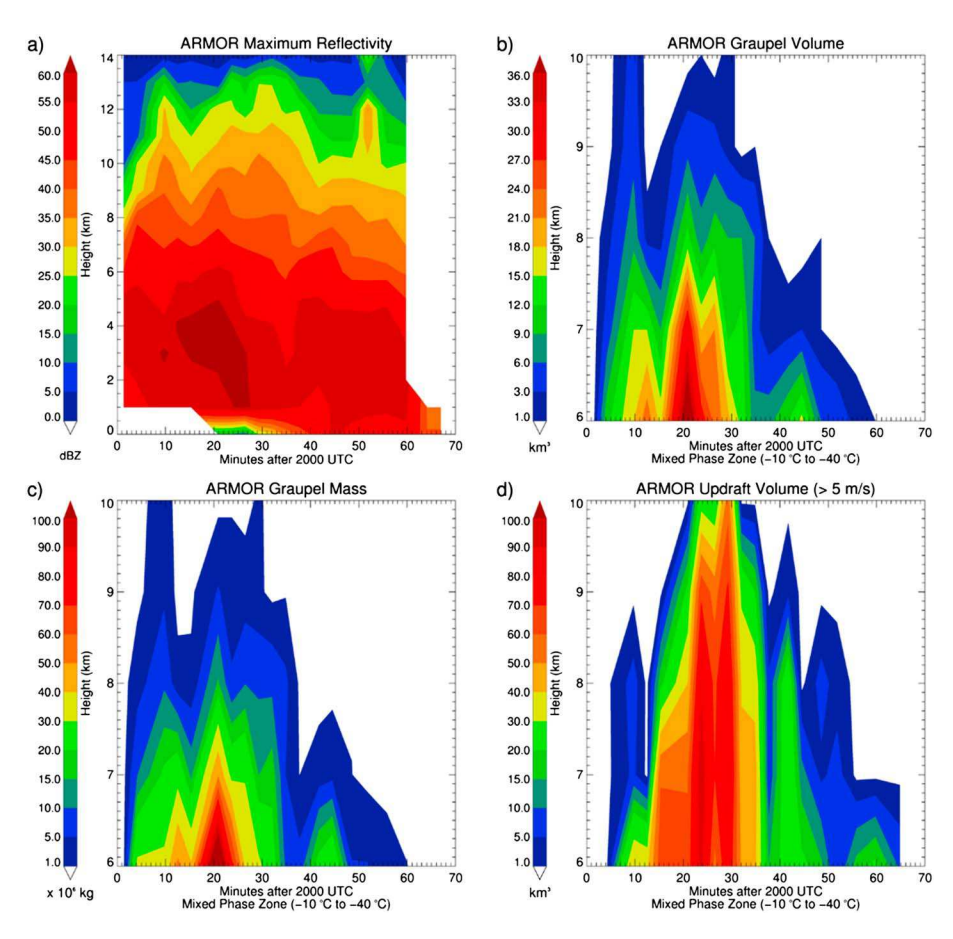


Figure 4. Time-height cross sections of radar microphysical and kinematic quantities associated with the multicell cluster on 21 May 2012. (a) Maximum reflectivity (dBZ, color shaded as shown), (b) graupel echo volume in the charging region (km³, color shaded as shown), (c) graupel mass in the charging region $(1 \times 10^6 \text{ kg}, \text{ color shaded as shown})$, and updraft volume $> 5 \text{ m s}^{-1} \text{ (km}^3, \text{ color shaded as shown})$. Time is in minutes after 2000 UTC.

The first radar-inferred pulse in the updraft volume, maximum reflectivity, and graupel echo volume and mass from 2001 to 2012 UTC is associated with the first SAD and LNO $_X$ production (Figure 3). A continued surge in the updraft up to its peak at ~2020 to 2030 UTC results in rapid coincident increases and maxima in the graupel echo volume and graupel mass. Likely associated with an explosion in the occurrence of graupel-ice collisions and charging, the total and IC lightning SAD also rapidly increase and peak at 2024 UTC (Figure 3c). The IC LNO $_X$ production also peaks at 2024 UTC (Figure 3d). However, the CG and total LNO $_X$ production (Figures 3b and 3f, respectively) both experience broad maxima between 2030 and 2045 UTC during which time the updraft volume, graupel volume, and graupel mass (Figure 4) are generally decreasing in the charging zone. As noted earlier, this period (2030–2045 UTC) is associated with CG flashes that initiate at >6 km altitude and have large extents and are sometimes referred to as IC-CG hybrid flashes in other studies [Matthee and Carey, 2014]. Secondary maxima in updraft volume, graupel volume, and mass after 2040 UTC are associated with secondary maxima in the SAD and LNO $_X$ production.

4.3. Time Series of LNOM Lightning Properties

IC flashes make up the overwhelming number of total lightning flashes as shown in the time series of flash rates in Figure 5. Both IC and total lightning activity begins around 2007 UTC and rapidly increases to a maximum around 2024 UTC. After 2024 UTC, the IC and total lightning flash activity decreases to a relative minimum around 2035–2038 UTC. Another relative maximum in IC and total lightning flash rate occurs at 2045 UTC. As also shown in Figure 5, the CG flash rate has no predominant peak (actual peak occurred at 2013 UTC) but remains fairly steady through most of the cluster lifecycle.

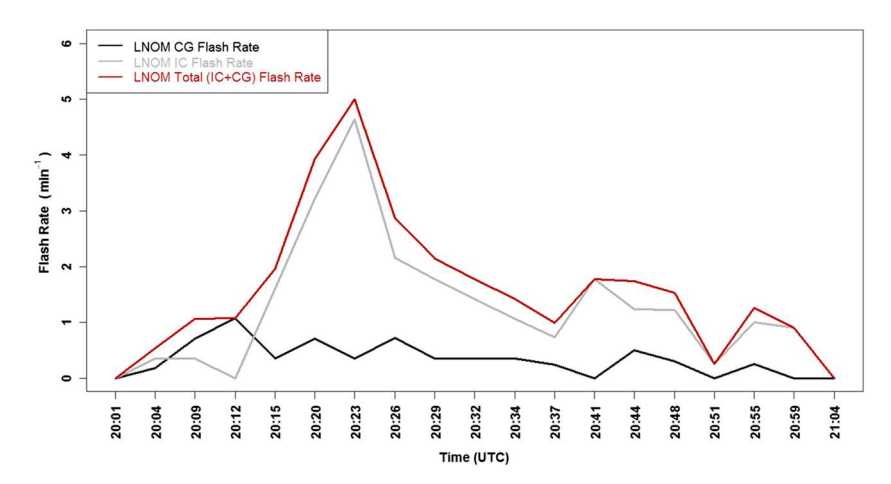


Figure 5. Time series of LNOM lightning flash rate for CG (black), IC (gray), and total (IC+CG) flashes (red).

The average LNOM flash extent (Figure 6a) increases during the ramp up in the flash rate (Figure 5) associated with the convective updraft. However, the average flash extent (which is the sum of all the flash extents per flash type over the radar volume time divided by the number of flashes per flash type that occurred during the radar volume time) lags the flash rate and both properties are somewhat anticorrelated (cf. Figures 5 and 6a). This was also found in MEA15 where flash rate and flash size (as calculated from a convex hull area, which is not the same as the extent discussed here) were anticorrelated. The largest average flash extents tend to occur after the maximum flash rate associated with the convective updraft (cf. MEA15). Late in the storm lifecycle, relative maxima in flash rate tend to be associated with relative minima in the flash extent (e.g., see 2045 UTC) and vice versa (e.g., see 2052 UTC), as also observed by MEA15.

The summed flash extent (i.e., the sum of lightning extent for all flashes during a given time period) is provided in Figure 6b. The summed flash extent for all flashes (i.e., IC + CG) is dominated largely by the summed flash extent of IC flashes, which is due to the much larger IC flash rates (Figure 5) and somewhat similar average flash sizes (Figure 6a). The time-averaged IC flash extent (not the summed flash extent) is 135.2 km while the time-averaged CG flash extent is 103.8 km. Meanwhile, the IC to CG ratio (IC:CG) is 3.7. Overall, the trend in the summed extent of lightning flashes is largely controlled by flash rate and not so much by average flash

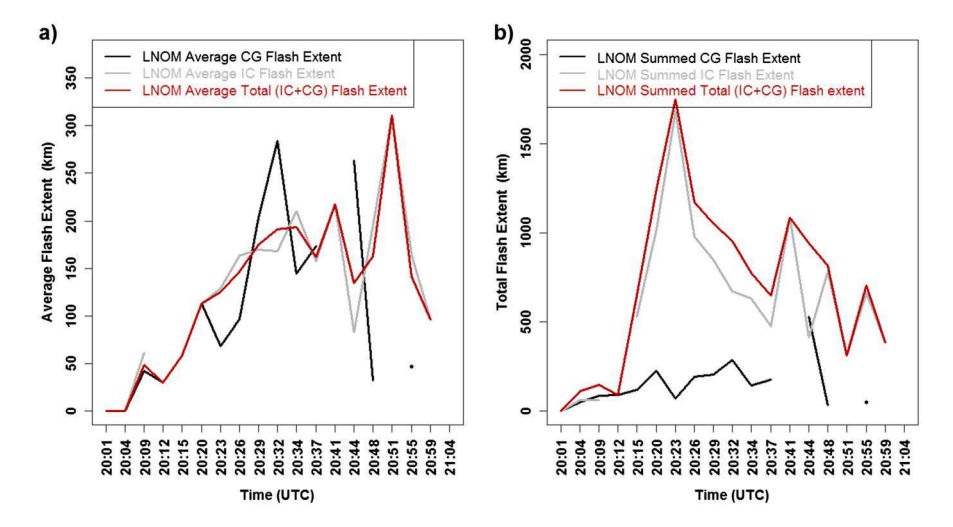


Figure 6. Time series of LNOM for the (a) average lightning flash extent (km) and (b) summed lightning flash extent, for CG (black), IC (gray), and total (IC + CG) flashes (red). The breaks in the results are because either no IC or CG flashes were recorded in that time frame; therefore, there were no flash extents calculated for these flash types at the specific times indicated (e.g., at 2051 and 2059 UTC for CG flashes). In order to make the results more evident, the "zero" values were removed and displayed as missing values, otherwise the results would be skewed toward smaller flash extents.

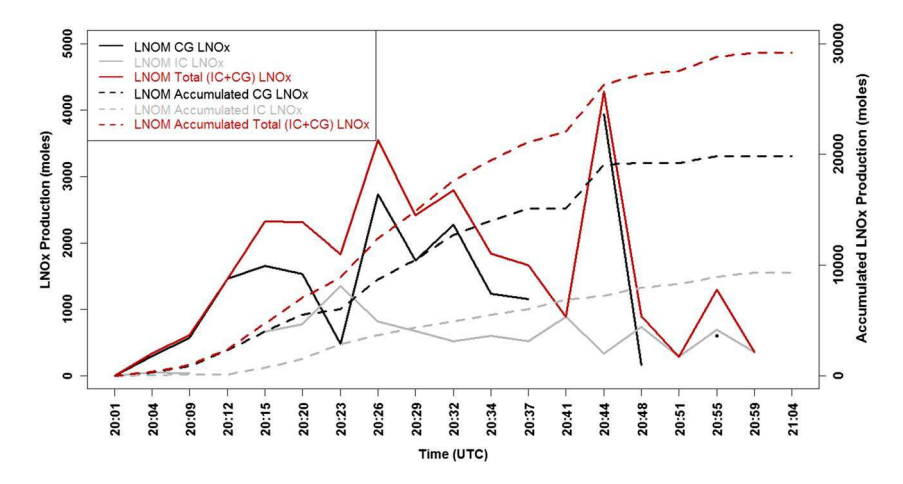


Figure 7. Time series of LNOM LNO $_X$ production (moles) for CG (black), IC (gray), and total (IC + CG) flashes (red). As in Figure 6, the breaks in the results are because either no IC or CG flashes were recorded in that time frame.

size (cf. Figures 5, 6a, and 6b). In fact, the Pearson correlation coefficient between the summed flash extent and flash rate is 0.87 for all flashes.

The time series of LNOM LNO $_X$ production as well as the accumulated LNO $_X$ production per flash type over time is shown in Figure 7. The majority of the accumulated LNO $_X$ production is due to the CG LNO $_X$ production, especially early in the storms' life cycle. On the other hand, the IC LNO $_X$ production is highly correlated to the summed IC flash extent (Figure 6b), which appears to be largely controlled by flash rate as noted above. More specifically, the Pearson correlation coefficient between IC LNO $_X$ production and summed IC flash extent is 0.99, which is to be expected given that the LNO $_X$ production parameterization scheme in *Koshak et al.* [2014] depends on channel length. Similarly, the Pearson correlation coefficient between

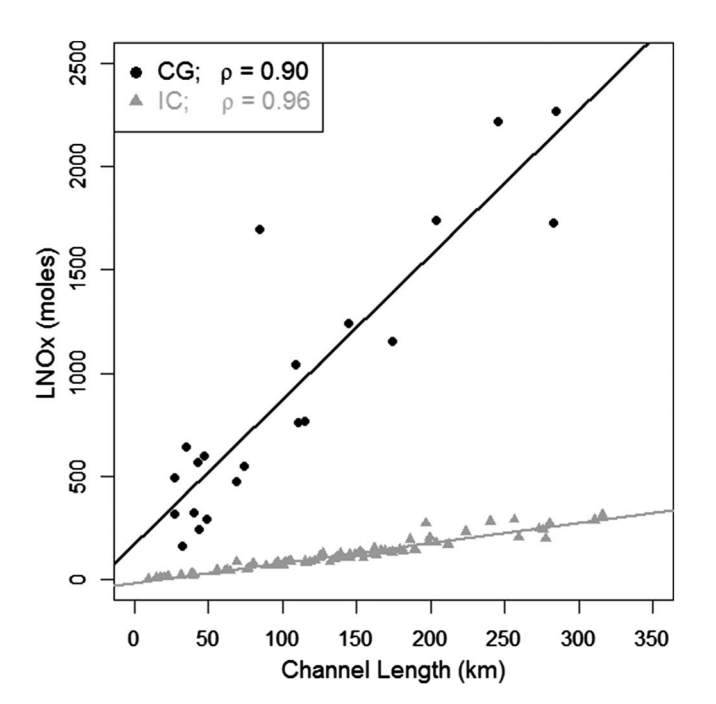


Figure 8. Correlation plot of LNO_X production (in moles) per flash type versus channel length (in km) per flash type. CG flash information is shown in black (filled circle and solid line, which is the best fit) while IC flash information is shown gray (triangles and solid line, which is the best fit).

CG LNO $_X$ production and the summed CG flash extent is 0.95. On the other hand, Figure 8 shows the Pearson correlation of LNO $_X$ production and channel length per flash type, indicating that for IC flashes, ρ = 0.96; while for CG flashes, ρ = 0.90. Therefore, the correlations are lower for both IC and CG flashes when one compares the per-flash results (Figure 8) to the summed results (Figure 7), indicating some variability on a per-flash basis.

As noted in *Koshak et al.* [2014], CG LNO_X production is governed in part by other CG flash parameters (e.g., peak current) in LNOM. Despite the fact that the summed IC flash extent is much larger than the summed CG flash extent (Figure 6b), the majority of LNO_X production is still from CG flashes (Figure 7). In other words, LNOM produces significantly more LNO_X on average for CG flashes (919 mol/flash) than for IC flashes (116 mol/flash) in this storm cluster.

This study

919

116

•	ible 1. Comparison of Moles of LNO _X per Flash Obtained by This LNOM Study to <i>Pickering et al.</i> [1998], <i>DeCaria et al.</i> [2005], Ott et al. [2007], Barthe and Barth [2008], and Koshak et al. [2014]				
Study	Differentiation of Flash Type	IC (moles per flash)	CG (moles per flash)		
Pickering et al. [1998]	Production of NO different for IC and CG	113	1113		
DeCaria et al. [2005]	Production of NO same for IC and CG	460	460		
Ott et al. [2007]	Production of NO same for IC and CG	360	360		
Barthe and Barth [2008]	Assumed all flashes were IC	121 ± 41	N/A		
Koshak et al. [2014]	Production of NO different for IC and CG	34.78	484.15		

Production of NO different for IC and CG

This result is largely traceable to the fact that CG flashes have larger currents (more energy for LNO_X production; Uman [1969]), longer channel lengths (including production from in-cloud IC components; Koshak [2014]), and lower located channel lengths (i.e., lower altitudes) where more air molecules are available for LNO_X production. These values compare well with those obtained by *Pickering et al.* [1998] but were lower (higher) than what was obtained by DeCaria et al. [2005] and Ott et al. [2007] for IC (CG) flashes and similar to Barthe and Barth's [2008] findings of IC flashes (see Table 1). This study also has higher LNO_X values per IC and CG flash as compared to Koshak et al. [2014]; however, Koshak et al. [2014] showed the average results for 27,873 IC flashes and 4832 CG flashes from several different thunderstorms that occurred during August over a 5 year period from 2005 to 2009 over North Alabama. Therefore, the results were representative of summer- to fall-type storms, whereas the storm analyzed in our study occurred during late spring-early summer. Finally, although LNOM transforms real and specific lightning observations into LNO_X production values, it is important to note that these values are still only estimates and as such are subject to further independent validation.

Figure 9 shows the LNOM lightning flash rate (the same as Figure 5) with a running mean of the LNO_X production per flash type. It is interesting to note that the LNO_X production per CG flash is larger from 2026 UTC to 2045 UTC (Figures 5 and 7-9) when the average CG flash extent is larger (Figure 6a). As noted earlier, many of these more extensive CG flashes are actually the hybrid IC-CG flashes noted in Matthee and Carey [2014]. This period also accounts for some of the largest CG and hence total flash LNO_X production for the storm cluster. From these results, we can conclude that the spatial extent of individual CG flashes can have a significant impact on the total LNO $_X$ production in a multicell storm cluster.

4.4. Comparison of LNOM and Radar Time Series

As stated earlier, in an effort to not repeat information shown in MEA15, the reader is referred to Figure 4 in this paper, as well as Figures 7 and 8 in MEA15, which shows the time series of radar-inferred kinematic and microphysical properties that are associated with the maximum updraft velocity and updraft volumes

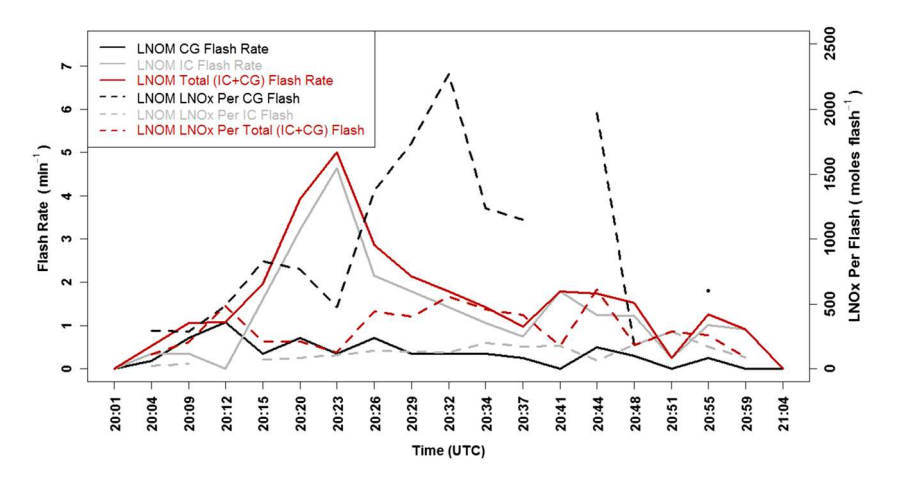


Figure 9. Time series of LNOM lightning flash rate for CG (black, solid lines), IC (gray, solid lines), and total flashes (red, solid lines); and the LNO_X production per flash type (i.e., running mean) for CG (black, striped lines), IC (gray, striped lines), and total (IC + CG) flashes (red, striped lines).

Table 2. Pearson Correlation Coefficient (ρ) Between the Time Series of Radar-Inferred Kinematic and Microphysical Quantities and LNOM Total (IC + CG) Lightning Properties for the Multicell Storm Cluster on 21 May 2012

Radar Parameter	Total Flash Rate (min ⁻¹)	Summed Flash Extent Rate (km min ⁻¹)	Total LNO χ Production (moles)
Graupel echo volume (km ³)	0.87	0.74	0.64
Graupel mass (kg)	0.85	0.63	0.50
Updraft volume (km ³)	0.81	0.81	0.55
Maximum updraft (m s ⁻¹)	0.77	0.61	0.54

(Figure 7 in MEA15), as well as the graupel mass and graupel volumes (Figure 8 in MEA15). By comparing the figures from MEA15 to Figures 4 and 6 in this paper, it is apparent that the flash rate increases along with the convective updraft and production of graupel in the charging zone, as has been seen in past studies. Rapid electrification and first lightning does not occur until after the maximum updraft in the charging zone exceeds 8 m s⁻¹ [e.g., *Zipser and Lutz*, 1994]. The graupel volume, graupel mass, updraft volume, and to a lesser extent, the maximum updraft are all reasonably well correlated to the total flash rate (Table 2) [e.g., CR96; CR00; *Wiens et al.*, 2005; *Deierling et al.*, 2008; *Deierling and Petersen*, 2008, MEA15]. For the most part, these radar parameters are not as well correlated (Table 2) with the summed flash extent rate (km min⁻¹) (which is the sum of the flash extent of all flashes (km) (Figure 6b) for a given radar sample period divided by the time period (min)), or the total (IC+CG) LNO_X production (mole) (Figures 6b and 7).

As stated in MEA15, the flash rates were well correlated to the maximum updraft speed, updraft volumes, graupel volume, and graupel mass (with correlations >0.88), but the flash sizes lagged the flash rate and the mentioned radar parameters. In fact, the flash sizes only increased rapidly *after* an increase in these radar parameters (MEA15). The same trends are seen in the LNOM analysis; flash sizes, and therefore LNO_X values, only increase after an increase in all the radar parameters as well as an increase in the flash rates. Therefore, including flash sizes as an LNO_X parameter, although important, is more complicated than for flash rates and it is not an easy one-to-one relationship between radar-derived parameters and flash sizes (or other LNO_X parameters) compared to the relationship between radar-derived parameters and flash rates. Further study is required using a variety of approaches (e.g., radar, lightning and aircraft observations, and modeling including with LNOM and WRF-Chem) in combination on a range of storm types to confirm the findings in Table 2 and firmly establish the relationships between kinematic and microphysical processes, flash properties, and LNO_X production.

5. Conclusions

This study has presented the first ever Lagrangian implementation of the NASA LNOM to study an individual storm (i.e., the LNOM cylindrical analysis domain was moved with the convection), allowing for a direct comparison between radar-inferred kinematic and microphysical properties and LNOM-inferred lightning flash and LNO $_X$ production characteristics. Although independent validation of the LNO $_X$ production estimates is still required, (therefore, the reader needs to use caution when applying the values presented in this document to their research), this study has demonstrated a useful new approach for combining radar observations, LMA observations, and a LNO $_X$ production model to better understand the kinematic and microphysical control of lightning properties and LNO $_X$ production in a variety of storms.

In order to explore the coevolving relationship between storm kinematics, microphysics, lightning properties, and LNO $_X$ production in ordinary convection, the NASA LNOM was applied to NALMA and NLDN lightning observations and compared to multi-Doppler and polarimetric radar observations of a multicell thunderstorm on 21 May 2012 (1953–2104 UTC) over northern Alabama during DC3. One of the most striking findings of this study is the relatively reduced correlation between LNO $_X$ production and updraft or graupel volume (correlation coefficient, ρ = 0.50 to 0.64) as compared to the higher correlation between those radar-inferred kinematic and microphysical properties and flash rate (ρ = 0.77 to 0.87). If this result is confirmed in a variety of storms and independently validated, then it might suggest that storm updraft and graupel volume (and other related kinematic and microphysical properties) may not be as accurate as originally thought as proxies for LNO $_X$ production in numerical cloud models. This suggestion is at odds with a variety of prior results and therefore requires further investigation and substantiation.



One of the primary factors that resulted in the decreased correlation between updraft/graupel volume and LNO_X production is the significantly larger average $LNOM LNO_X$ per flash production for CG flashes than for IC flashes in this specific multicell convection. If the average LNO_X production for CG and IC flashes had been more similar, then we speculate that the correlation between updraft/graupel volume and LNO_X production would have been higher. This speculation is based on the fact that (1) IC flashes dominated both flash rate and extent and (2) updraft/graupel volume was better correlated to IC flash rate, extent and LNO_X production and less well correlated to CG flash rate, extent and LNO_X production in this storm (cf. Figures 3 and 4).

Clearly, more research is required to resolve these issues. In particular, we recommend that future research should prioritize running LNOM on a variety of storm types in a variety of different environments that include radar, LMA and in situ observations. It is particularly important to study one or more cases in which a variety of approaches for estimating LNO_X production can be compared and contrasted, potentially including (1) WRF-Chem modeling (2) in situ measurements, and (3) radar lightning observations combined with LNOM.

The key findings of the study are summarized as follows:

- 1. The total (IC + CG) and IC flash SADs are very similar with a dominant peak at 8 to 10 km and a less pronounced shelf at 6 km. The IC flash SAD comprises a significant fraction of the total SAD. The CG flash SAD is significantly smaller, somewhat multimodal with a dominant peak between 4 and 6 km altitude. In an absolute sense, the IC SAD dominates at all vertical levels except below 3 km.
- 2. Despite dominating the SAD, the IC flash LNO_X production peak at 8 km is less than the corresponding CG flash LNO_X production peak at 6 km. The CG LNO_X production is generally larger than the IC LNO_X production at all altitudes less than 6 km while above that height the two production terms are comparable.
- 3. One notable trend in the CG flash activity is the increase in CG flash SAD in the charging zone aloft at altitudes >6 km *after* the simultaneous peaks in the total and IC lightning flash rate, graupel volume/mass and convective updraft volume at 2024 UTC, which are all associated with a convective pulse. A large number of the LNOM CG flashes (i.e., associated with NLDN CG flash) during this time when the convective updraft is weakening are categorized as IC-CG hybrid flashes because the VHF sources start at >6 km altitude and have large extents aloft before coming to ground (MEA15).
- 4. At heights below 6 km, the CG LNO_X production dominates the column integrated LNO_X production associated with all flashes. Unlike SAD, total LNO_X production is a more equal contribution of both IC and CG LNO_X production terms at heights above 6 km. Overall, column integrated CG LNO_X production dominates the column integrated total LNO_X production associated with all flashes with both quantities peaking *after* the simultaneous peaks in the convective updraft volume, graupel volume, and flash rate.
- 5. The first radar inferred pulse in the updraft volume, maximum updraft, maximum reflectivity, and graupel volume/mass precede the first lightning flash and associated LNO_X production. Graupel volume/mass, updraft volume, and to a lesser extent maximum updraft are all reasonably well correlated to the LNOM total flash rate.
- 6. The CG and total LNO_X production both experience maxima after the peak in the convective activity when the updraft volume, graupel volume/mass are generally decreasing in the charging zone. These radar kinematic and microphysical parameters associated with the convective activity are not as well correlated to the summed flash extent or the total LNO_X production as they are to flash rates.
- 7. The average LNOM flash extent ramps up during the increase in the flash rate. However, the average flash extent lags the flash rate and both properties are somewhat anticorrelated (the same was found in MEA15, although a different flash rate and flash size calculation were used). The largest average flash extents tend to occur *after* the maximum flash rate associated with the convective updraft.
- 8. Overall, the summed flash extent of lightning flashes is largely controlled by total (IC+CG) flash rate and not so much by average flash size. This result may be specific to ordinary multicell convection and more work is required to investigate this relationship in other storm types (e.g., supercells and mesoscale convective systems).
- 9. As expected, given that the parameterization of LNO_X within LNOM depends in part on channel length, the IC LNO_X production is highly correlated to the summed IC flash extent (ρ = 0.99), which is strongly controlled by flash rate in this storm; while ρ = 0.96 per IC flash. Similarly, the correlation between CG LNO_X production and the summed CG flash extent is 0.95; while ρ = 0.90 per CG flash.



- 10. Despite the fact that the summed IC flash extent is much larger than the summed CG flash extent, the majority of LNO_X production is still from CG flashes. In other words, LNOM produces significantly more LNO_X on average for CG flashes (919 mol/flash) than for IC flashes (116 mol/flash) in this multicell convection.
- 11. The LNO_x production per CG flash is larger from 2026 to 2045 UTC when the average CG flash extent is larger. As noted earlier (see point 5), many of these extensive CG flashes are actually hybrid IC-CG flashes with large extents at heights above 6 km. This period accounts for some of the largest CG and hence total (IC + CG) flash LNO_x production for the storm. Since the CG flashes were small in number, the extent of individual CG flashes can have a significant impact on total LNO_{χ} production.

Acknowledgments

We wish to recognize funding from the National Science Foundation's Physical and Dynamical Meteorology (NSF PDM) Program (AGS-1063573), which has supported the DC3 field experiment and associated research. We want to acknowledge Lamont Bain for his time editing and gridding the ARMOR and KHTX data and for creating the dual-Doppler fields used in this and other manuscripts. We also wish to thank the many, many people who made the collection of DC3 observations possible. The data used herein can be obtained from the DC3 webpage located here: http://data.eol.ucar.edu/master list/? project=DC3. Finally, we wish to thank three anonymous reviewers for comments that have substantially improved the quality of this research paper.

References

- Bain, A. L. (2013), Polarimetric Doppler radar and electrical observations of deep moist convection across northern Alabama during the deep convective clouds and chemistry experiment, MS thesis, 148 pp., Dep. of Atmospheric Sciences, Univ. of Alabama in Huntsville.
- Bain, A. L., R. Matthee, and L. D. Carey (2013). Polarimetric radar and electrical observations of deep moist convection across northern Alabama during the DC3 experiment, paper presented at AMS 36th Conference on Radar Meteorology, September 16-20, Breckenridge,
- Barth, M. C., et al. (2015), The deep convective clouds and chemistry (DC3) field campaign, Bull. Am. Meteorol. Soc., 96, 1281–1309, doi:10.1175/BAMS-D-13-00290.1.
- Barthe, C., and M. C. Barth (2008), Evaluation of a new lightning-produced NO_X parameterization for cloud resolving models and its associated uncertainties, Atmos. Chem. Phys., 8, 4691-4710.
- Barthe, C., W. Deierling, and M. C. Barth (2010), Estimation of total lightning from various storm parameters: A cloud-resolving model study, J. Geophys. Res., 115, D24202, doi:10.1029/2010JD014405.
- Bringi, V. N., K. Knupp, A. Detwiler, L. Liu, I. J. Caylor, and R. A. Black (1997), Evolution of a Florida thunderstorm during the convection and precipitation/electrification experiment: The case of 9 August 1991, Mon. Weather Rev., 125, 2131–2160, doi:10.1175/1520-0493(1997) 125,2131:EOAFTD.2.0.CO;2.
- Bruning, E. C., and D. R. MacGorman (2013), Theory and observations of controls on lightning flash size spectra, J. Atmos. Sci., 70, 4012-4029.
- Carey, L. D., and S. A. Rutledge (1996), A multiparameter radar case study of the microphysical and kinematic evolution of a lightning producing storm, J. Meteorol, Atmos. Phys., 59, 33-64.
- Carey, L. D., and S. A. Rutledge (2000), The relationship between precipitation and lightning in tropical island convection: A C-Band polarimetric radar study, Mon. Weather Rev., 128, 2687-2710.
- Carey, L. D., M. J. Murphy, T. L. McCormick, and N. W. S. Demetriades (2005), Lightning location relative to storm structure in a leading-line, trailing-stratiform mesoscale convective system, J. Geophys. Res., 110, D03105, doi:10.1029/2003JD004371.
- Chronis, T., T. Lang, W. Koshak, R. Blakeslee, H. Christian, E. McCaul, and J. Bailey (2015), Diurnal characteristics of lightning flashes detected over the São Paulo lightning mapping array, J. Geophys. Res. Atmos., 120, 11,799–11,808, doi:10.1002/2015JD023960.
- Cooray, V., M. Rahman, and V. Rakov (2009), On the NO_X production by laboratory electrical discharges and lightning, J. Sol. Atmos. Terr. Phys., *71*, 1877–1889.
- Cooray, V., M. Rahman, and V. Rakov (2012), On the NOx production by laboratory electrical discharges and lightning, in Lightning Electromagnetics, edited by V. Cooray, The Institution of Engineering and Technology (IET – former IEE), London.
- DeCaria, A. J., K. E. Pickering, G. L. Stenchikov, J. R. Scala, J. L. Stith, J. E. Dye, B. A. Ridley, and P. Laroche (2000), A cloud-scale model study of lightning-generated NO_X in an individual thunderstorm during STERAO-A, J. Geophys. Res., 105, 11,601–11,616, doi:10.1029/ 2000JD900033.
- DeCaria, A. J., K. E. Pickering, G. L. Stenchikov, and L. E. Ott (2005), Lightning-generated NO_X and its impact on tropospheric ozone production: A three-dimensional modeling study of a stratosphere-troposphere experiment: Radiation, aerosols and ozone (STERAO-A) thunderstorm, J. Geophys. Res., 110, D14303, doi:10.1029/2004JD005556.
- Deierling, W., and W. A. Petersen (2008), Total lightning activity as an indicator of updraft characteristics, J. Geophys. Res., 113, D16210, doi:10.1029/2007JD009598.
- Deierling, W., W. A. Petersen, J. Latham, S. Ellis, and H. J. Christian (2008), The relationship between lightning activity and ice fluxes in thunderstorms, J. Geophys. Res., 113, D15210, doi:10.1029/2007JD009700.
- Dye, J. E., J. J. Jones, W. P. Winn, T. A. Cerni, B. Gardiner, D. Lamb, R. L. Pitter, J. Hallett, and C. P. R. Saunders (1986), Early electrification and precipitation development in a small, isolated Montana cumulonimbus, J. Geophys. Res., 91, 1231–1247, doi:10.1029/JD091iD01p01231.
- Dye, J. E., W. P. Winn, J. J. Jones, and D. W. Breed (1989), The electrification of New Mexico thunderstorms. I. Relationship between precipitation development and the onset of electrification, J. Geophys. Res., 94, 8643–8656, doi:10.1029/JD094iD06p08643.
- Dye, J. E., et al. (2000), An overview of the stratospheric-tropospheric experiment: Radiation, aerosols, and ozone (STERAO)-deep convection experiment with results for the July 10, 1996 storm, J. Geophys. Res., 105, 10,023-10,045, doi:10.1029/1999JD901116.
- Fehr, T., H. Höller, and H. Huntrieser (2004), Model study on production and transport of lightning-produced NO_X in a EULINOX supercell storm, J. Geophys. Res., 109, D09102, doi:10.1029/2003JD003935.
- Gallardo, L., and V. Cooray (1996), Could cloud-to-cloud discharges be as effective as cloud-to-ground discharges in producing NOx?, Tellus, 48B, 641-651.
- Gallardo, L., and H. Rodhe (1997), Oxidized nitrogen in the remote Pacific: The role of electrical discharges over the oceans, J. Atmos. Chem., 26, 147-168.
- Goodman, S. J., D. E. Buechler, P. D. Wright, and W. D. Rust (1988), Lightning and precipitation history of a microburst-producing storm, Geophys. Res. Lett., 15, 1185-1188, doi:10.1029/GL015i011p01185.
- Goodman, S. J., et al. (2005), The North Alabama lightning mapping array: Recent severe storm observations and future prospects, Atmos. Res., 76, 423-437.
- Jameson, A. R., M. J. Murphy, and E. P. Krider (1996), Multiple parameter radar observations of isolated Florida thunderstorms during the onset of electrification, J. Appl. Meteorol., 35, 343-354, doi:10.1175/1520-0450(1996)035,0343:MPROOI.2.0.CO;2.



- Koshak, W., H. Peterson, A. Biazar, M. Khan, and L. Wang (2014), The NASA lightning oxides model (LNOM): Application to air quality modeling, Atmos. Res., 135-136, 363-369.
- Koshak, W. J. (2014), Global Lightning Nitrogen Oxides Production, 2nd ed., edited by V. Cooray, chap. 19, 928 pp., Springer, Netherlands. Koshak, W. J., et al. (2004), North Alabama Lightning Mapping Array (LMA): VHF source retrieval algorithm and error analyses, J. Atmos. Oceanic Technol., 21, 543-558.
- Koshak, W. J., R. J. Solakiewicz, and H. S. Peterson (2015), A return stroke NO_x production model, J. Atmos. Sci., 72(2), 943–954.
- Kuhlman, K. M., D. R. MacGorman, M. I. Biggerstaff, and P. R. Krehbiel (2009), Lightning initiation in the anvils of two supercell storms. Geophys. Res. Lett., 36, L07802, doi:10.1029/2008GL036650.
- Lang, T. J., and S. A. Rutledge (2002), Relationships between convective storm kinematics, precipitation, and lightning, Mon. Weather Rev., 130, 2492-2506, doi:10.1175/1520-0493(2002)130,2492:RBCSKP.2.0.CO;2.
- Li, Y., K. E. Pickering, M. C. Barth, M. M. Bela, K. Cummings, D. J. Allen, L. D. Carey, G. S. Diskin, T. L. Campos, and A. O. Fierro (2014), An analysis of deep convective transport in May 21, 2012 DC3 Alabama thunderstorms using results from WRF-Chem simulations, Poster, Abstract A53C-3237 presented at 2014 Fall Meeting, AGU, San Francisco, Calif., 15-19 Dec.
- Li, Y., K. E. Pickering, M. C. Barth, M. M. Bela, K. Cummings, D. J. Allen, L. D. Carey, R. M. Mecikalski, A. Fierro, and G. Mullendore (2016), Deep convective transport in convective systems of three different scales from the DC3 field campaign using results from WRF-Chem simulations with lightning data assimilation, Recorded presentation, 2016 AMS / 18th Conference on Atmospheric Chemistry, New Orleans, La. 10-15 Jan.
- Matthee, R., and L. Carey (2014), Storm physics and lightning properties over Northern Alabama during DC3, XV International Conference on Atmospheric Electricity, 15-20 June 2014, Norman, Okla.
- McCaul, E. W., Jr., J. C. Bailey, J. Hall, S. J. Goodman, R. J. Blakeslee, and D. E. Buechler (2005), A flash clustering algorithm for North Alabama Lightning Mapping Array data, Conf. on Meteorological Applications of Lightning Data, San Diego, Calif., Amer. Meteor. Soc., 5.3. [Available at https://ams.confex.com/ams/Annual2005/techprogram/paper_84373.htm.]
- Mecikalski, R. M., A. L. Bain, and L. D. Carey (2015), Radar and lightning observations of deep moist convection across northern Alabama during DC3: 21 May 2012, Mon. Weather Rev., 143(7), 2774-2794, doi:10.1175/MWR-D-14-00250.1.
- Miller, L. J., and T. Frederick (1998), Custom editing and display of reduced information in Cartesian space, technical report published by the National Center For Atmospheric Research (NCAR), Mesoscale and Microscale Meteorology Division, June 1998, available at NCAR Earth Observation Laboratory's Radar Data Analysis Tools. [Available at https://wiki.ucar.edu/display/raygridding/home.]
- Ott, L. E., K. E. Pickering, G. Stenchikov, H. Huntrieser, and U. Schumann (2007), Effects of lightning NO_X production during the 21 July European Lightning Nitrogen Oxides Project storm studied with a three-dimensional cloud-scale chemical transport model, J. Geophys. Res., 112, D05307, doi:10.1029/2006JD007365.
- Ott, L. E., K. E. Pickering, G. L. Stenchikov, A. J. DeCaria, R.-F. Lin, D. Wang, S. Lang, and W.-K. Tao (2010), Production of lightning NOx and its vertical distribution calculated from 3-D cloud-scale transport model simulations, J. Geophys. Res., 115, D04301, doi:10.1029/2009JD011880.
- Petersen, W. A., et al. (2005), The UAH-NSSTC/WHNT ARMOR C-band Dual-Polarimetric Radar: A unique collaboration in research, education and technology transfer, paper presented at AMS 32nd Radar Meteorology Conference, Albuquerque, New Mexico.
- Peterson, H., M. Bailey, J. Hallett, and W. Beasley (2009), NO_x production in laboratory discharges simulating blue jets and red sprites, J. Geophys. Res., 114, A00E07, doi:10.1029/2009JA014489.
- Peterson, H., M. Bailey, J. Hallett, and W. Beasley (2010), Reply to "Comment on 'NO_X production in laboratory discharges simulating blue jets and red sprites", J. Geophys. Res., 115, A12306, doi:10.1029/2010JA015946.
- Pickering, K. E., Y. Wang, W. K. Tao, C. Price, and J.-F. Müller (1998), Vertical distributions of lightning NO_X for use in regional and global chemical transport models, J. Geophys. Res., 103, 31,203-31,216, doi:10.1029/98JD02651.
- Pollack, I. B., et al. (2016), Airborne quantification of upper tropospheric NO_X production from lightning in deep convective storms over the United States Great Plains, J. Geophys. Res. Atmos., 121, 2002-2028, doi:10.1002/2015JD023941.
- Price, C., J. Penner, and M. Prather (1997), NO_X from lightning. 1. Global distribution based on lightning physics, J. Geophys. Res., 102, 5929-5941, doi:10.1029/96JD03504.
- Ridley, B. A., K. E. Pickering, and J. E. Dye (2005), Comments on the parameterization of lightning-produced NO in global chemistry transport models, Atmos. Environ., 39, 6184-6187.
- Saunders, C. P. R. (1994), Thunderstorm electrification laboratory experiments and charging mechanisms, J. Geophys. Res., 99, 10,773–10,779, doi:10.1029/93JD01624.
- Saunders, C. P. R., and S. L. Peck (1998), Laboratory studies of the influence of the rime accretion rate on charge transfer during crystal/graupel collisions, J. Geophys. Res., 103, 13,949-13,956, doi:10.1029/97JD02644.
- Schultz, C. J., L. D. Carey, E. V. Schultz, and R. J. Blakeslee (2015), Insight into the physical and dynamical processes that control lightning jumps, Weather Forecasting, 30, 1591-1621, doi:10.1175/WAF-D-14-00147.1.
- Schumann, U., and H. Huntrieser (2007), The global lightning-induced nitrogen oxides source, Atmos. Chem. Phys., 7, 382-3907.
- Straka, J. M., D. S. Zrnić, and R. V. Ryzhkov (2000), Bulk hydrometeor classification and quantification using polarimetric radar data: Synthesis of relations, J. Appl. Meteorol., 39, 1341-1372.
- Takahashi, T. (1978), Riming electrification as a charge generation mechanism in thunderstorms, J. Atmos. Sci., 35, 1536–1548, doi:10.1175/ 1520-0469(1978)035,1536:REAACG.2.0.CO;2.
- Thomas, R., P. Krehbiel, W. Rison, J. Harlin, T. Hamlin, and N. Campbell (2003), The LMA flash algorithm, Proc. 12th Int. Conf. On Atmospheric Electricity, Versailles, France, International Commission on Atmospheric Electricity, 655 - 656.
- Uman, M. (1969), Lightning, McGraw-Hill, New York.
- Vivekanandan, J., D. S. Zrnić, S. Ellis, R. Oye, and A. V. Ryzhkov (1999), Cloud microphysics retrievals using S-Band dual-polarization radar measurements, Bull. Am. Meteorol. Soc., 80, 381-388.
- Wang, Y., A. W. DeSilva, and G. C. Goldenbaum (1998), Nitric oxide production by simulated lightning: Dependence on current, energy and pressure, J. Geophys. Res., 103(D15), 19,149-19,159, doi:10.1029/98JD01356.
- Weiss, S. A., D. R. MacGorman, and K. M. Calhoun (2012), Lightning in the anvils of supercell thunderstorms, Mon. Weather Rev., 140, 2064-2079
- Wiens, K. C., S. A. Rutledge, and S. A. Tessendorf (2005), The 29 June 2000 supercell observed during STEPS. Part II: Lightning and charge structure, J. Atmos. Sci., 62, 4151-4177.
- Zipser, E. J., and K. R. Lutz (1994), The vertical profile of radar reflectivity of convective cells: A strong indicator of storm intensity and lightning probability?, Mon. Weather Rev., 122, 1751-1759.